JACS
JOURNAL OF THE AMERICAN CHEMICAL SOCIETY

ARTICLE

pubs.acs.org/JACS

# Atomistic Simulation of Cholesterol Effects on Miscibility of Saturated and Unsaturated Phospholipids: Implications for Liquid-Ordered/Liquid-Disordered Phase Coexistence

Jason de Joannis,[†,‡] Patrick S. Coppock,[†,⊥] Fuchang Yin,[†] Makoto Mori,[†] Absalom Zamorano,[†,#] and James T. Kindt*[,†]

[†]Cherry L. Emerson Center for Scientific Computation and Department of Chemistry, Emory University, Atlanta, Georgia 30322, United States

[#]Institutional Program of Molecular Biomedicine, ENMH-IPN, Mexico City, Mexico

Supporting Information

**ABSTRACT:** Mixed MD/MC simulation at fixed difference in chemical potential ($\Delta\mu$) between two lipid types provides a computational indicator of the relative affinities of the two lipids for different environments. Applying this technique to ternary DPPC/DOPC/cholesterol bilayers yields a DPPC/DOPC ratio that increases with increasing cholesterol content at fixed $\Delta\mu$, consistent with the known enrichment of DPPC and cholesterol-rich in liquid-ordered phase domains in the fluid−fluid coexistence region of the ternary phase diagram. Comparison of the cholesterol-dependence of PC compositions at constant $\Delta\mu$ with experimentally measured coexistence tie line end point compositions affords a direct test of the faithfulness of the atomistic model to experimental phase behavior. DPPC/DOPC ratios show little or no dependence on cholesterol content at or below 16% cholesterol in the DOPC-rich region of the composition diagram, indicating cooperativity in the favorable interaction between DPPC and cholesterol. The relative affinity of DPPC and DOPC for high cholesterol bilayer environments in simulations is explicitly shown to depend on the degree of cholesterol alignment with the bilayer normal, suggesting that a source of the cooperativity is the composition dependence of cholesterol tilt angle distributions.

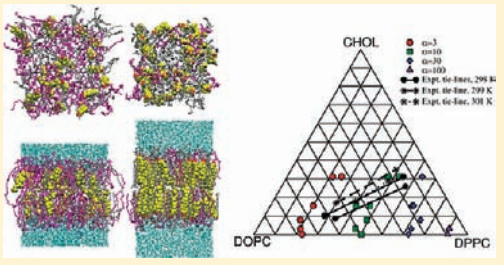


## INTRODUCTION

The importance of cholesterol, a major component of eukaryotic membranes, in modulating membrane properties has been studied extensively. The observation of domains enriched in cholesterol along with certain sphingo- and phospholipid types, first in detergent-solubilized membranes, has sparked an entire subfield of membrane biophysics devoted to the detection and characterization of such domains in vivo and in model systems.[1−6] The phase diagrams of several ternary bilayer systems, each a mixture of two bilayer-forming lipids with added cholesterol, have been subject to careful experimental scrutiny;[7−12] several have yielded coexisting "liquid-ordered" (LO) domains (rich in cholesterol and the higher-melting lipid component) and "liquid-disordered" (LD) domains (rich in the lower-melting lipid component).

The degree of lateral order within these phases, the precise nature of the driving force behind the phase separation, and the extent to which the LO phases correspond to domains present in vivo[5] remain areas of intense experimental, theoretical, and computational study. Different pieces of the overall picture have been explained using models that contain different levels of complexity. The overall phase behavior can be modeled by assuming that the free energies of interactions between cholesterol and neighboring lipids are very different, and that the lipids themselves mix nonideally.[13] An "umbrella model" provides a qualitative explanation for the ordering effect of cholesterol on lipid tail chains, whereby the inclusion of cholesterol (with its small polar headgroup area) lowers the overall area/volume ratio of the bilayer and drives a compensatory thickening of the bilayer accompanied by an extension of lipid tails to shield the hydrophobic cholesterol body.[14] Some experimental studies of cholesterol-containing monolayers and bilayers have suggested that cholesterol associates with saturated-tail lipids in well-defined stoichiometric ratios, consistent with geometrically precise superlattice structures.[15,16] The underlying interactions that produce such structures can be modeled by two-dimensional lattice models that explicitly include many-body effects.[17] Field-theoretic approaches represent the system by assigning values for the local order and composition as functions of lateral position. These properties are evolved under the influence of free energy functions derived from molecular representations of the lipids and cholesterol, which may be lattice-based or atomistic.[18,19] Such approaches capture the coupling of lipid tail ordering and phase separation. Coarse-grained models of cholesterol-containing bilayers have also been used extensively for insight into effects that develop over longer times and greater length scales,

**Received:** November 19, 2010
**Published:** February 22, 2011

ACS Publications © 2011 American Chemical Society

particularly the coupling of domain structures between leaflets and the coupling of domain positioning with local curvature.[20−22]

Atomistic (or united-atom) simulation studies have been used to obtain fully detailed pictures of the striking effects of cholesterol on bilayer structures for over a decade.[23] Important structural insights have been obtained so far, including rationalizations for why cholesterol leads to a more ordered bilayer when some related sterols do not.[24−27] Differences in molecular packing can be analyzed for insight into the relative affinities of various lipid tails for cholesterol.[28] Effects of cholesterol orientation have been discussed extensively, with some reports emphasizing the anisotropy of the interactions of the "rough" (methylated) and "smooth" faces of cholesterol[19,29,30] and others focused on the cholesterol tilt angle with respect to the bilayer normal.[27,31,32] The connection between the azimuthal and axial rotational degrees of freedom has been explored through simulations of bilayers containing a "smooth" cholesterol analogue, which showed a broader distribution of tilt angles than native cholesterol.[33]

The actual phenomenon of phase separation cannot, however, be seen over the time- and length-scales of simulations currently feasible at the atomistic level, although preliminary reorganizations are evident in long (>100 ns) trajectories of ternary systems.[29,34] Except for recent studies aimed at calculating free energies associated with insertion or removal of cholesterol[35] or phospholipids[36] into the bilayer, atomistic simulation studies have not been in position to address the thermodynamic (as opposed to structural) aspects of mixing and demixing in these complex systems. Developing the means to evaluate the tendency of an atomistic model system to undergo phase separation is very desirable for several purposes: to directly test the model's faithfulness to experimental phase behavior, to probe mechanistic hypotheses about factors that contribute to phase separation, and ultimately to predict the sensitivity of the phase separation phenomenon to molecular structure and other environmental factors.

In the present study, isomolar semigrand canonical ensemble simulations, performed at fixed difference in chemical potential $\Delta\mu_{DPPC-DOPC}$, have been performed to assess the tendency of DPPC and DOPC to demix in the presence of cholesterol. This method has previously been applied to study phase coexistence between gel and fluid phases in binary mixed bilayers[37] and to study tail-length-dependent local demixing in mixed bilayers associated with edges,[38] pores,[39] and transmembrane peptides.[40] The current results allow for the first time a direct (although incomplete) quantitative comparison between atomistic simulation results and the experimental phase diagram of the ternary system. The comparison is possible because at equilibrium, each component of two coexisting phases has the same chemical potential $\mu$ in one phase as in the other. In the phase-separating ternary systems of interest, therefore, the difference $\Delta\mu_{DPPC-DOPC} = \mu_{DPPC} - \mu_{DOPC}$ must be the same in the cholesterol-rich LO phase as in the cholesterol-poor LD phase, even though the ratio of DPPC to DOPC differs. Each pair of end points of experimental tie lines on the ternary phase diagram, which represent compositions of phases at equilibrium, must lie on a unique curve of constant $\Delta\mu_{DPPC-DOPC}$. If the demixing behavior of the simulation model is faithful to experiment, curves generated from simulations at constant $\Delta\mu_{DPPC-DOPC}$ but varying cholesterol content should therefore run parallel to experimental tie lines on the ternary phase diagram. Within a system, furthermore, each lipid undergoes mutation moves that are subject to the influences of the local environment, as the success probability of any mutation depends not only on $\Delta\mu_{DPPC-DOPC}$ but also on the relative stability of the originial and mutated structures. Therefore, any equilibrium nonuniformity in the lateral distribution of DPPC and DOPC will approach equilibrium much faster than it would through diffusive mixing. For instance, if proximity to cholesterol favors DPPC relative to DOPC, this preference will tend to emerge from the simulations as a greater-than-average occupancy of sites near cholesterol by DPPC, because the enhanced stability of DPPC will enhance the success probability of mutation attempts from DOPC to DPPC at those sites and/or decrease the probability of the reverse mutations.

The present simulations demonstrate that a commonly used united-atom simulation model captures cholesterol's higher affinity for DPPC than for DOPC, as the DPPC/DOPC ratio increases with increasing cholesterol content at fixed $\Delta\mu_{DPPC-DOPC}$, but with a slightly weaker tendency to demix than seen in experiment. The observed dependence of composition on cholesterol content at fixed $\Delta\mu_{DPPC-DOPC}$ over a broad expanse of the phase diagram is qualitatively different from predictions of simple nearest-neighbor attraction models and indicates that cholesterol only exhibits a preference for DPPC under conditions of high enough cholesterol and/or DPPC content. A simple molecular interpretation of this cooperative behavior is that cholesterol's affinity for DPPC over DOPC depends on its alignment with the bilayer normal, with lower tilt angles promoted by cholesterol−cholesterol steric exclusion and by the tendency of DPPC tails to adopt extended conformations near its transition temperature. A direct test of this interpretation, using external fields to enhance or disrupt cholesterol orientational order, shows that tilt angle does influence the relative affinity of DPPC and DOPC for a cholesterol-rich environment, but leaves room for other contributions to cooperativity.

## METHODS

Conventional MD simulations were performed using Gromacs 3.3.1.[41] The Langevin thermostat, with a time constant of 0.2 ps, was used to maintain a constant temperature of 298 K in all simulations. All simulations were performed using periodic boundary conditions in three dimensions, with box dimensions scaled independently to maintain an average of 1.0 bar pressure in the plane of the bilayer and along the bilayer normal, with a time constant of 1.0 ps assuming a compressibility of $4.5 \times 10^{-5}$ bar$^{-1}$, using the Berendsen method.[42] A time step of 2 fs was used, and the LINCS[43] and SETTLE[44] algorithms were used to constrain all bonds to fixed lengths. The particle-mesh Ewald method, with Gromacs default parameters, was used for electrostatics.[45]

MCMD simulations were performed using GIMLi 1.0, a modified version of Gromacs that is available as a user contribution on the Gromacs Web site. During MCMD simulations, after every MD time step, a lipid (DPPC or DOPC) is chosen at random and subjected to a mutation move attempt using the configuration-bias algorithm.[46] The attempt consists of a regrowth of all segments below the ninth carbons of both lipid tails; the sites on the headgroup and the upper sections of the tails, whose interactions are identical in both lipids, are unchanged by the mutation. For each segment, a set of $k = 8$ possible positions are first generated using the appropriate fixed bond length and orientational probabilities weighted by the Boltzmann distribution for that segment's contribution to internal (bending and dihedral) potential energies. One out of the eight positions is then selected with a probability proportional to $\exp(-\beta U_{LJ})$, where $U_{LJ}$ represents the Lennard-Jones energy of interaction with all other sites in the system (up to a cutoff of $r = 1.0$ nm). Successive segments are generated until both tails are complete. (As a united-atom model was used for the tails, there is no Coulomb

**Table 1. MCMD Trajectories' Initial and Mean Compositions**

| run label[a] | $N_{PC}$ | $N_{Chol}$ | $N_{Sol}$ | $\alpha_{DPPC-DOPC}$ | $N_{DPPC}/N_{PC}$, initial | $t_{tot}$ (ns) | $\langle N_{DPPC}\rangle/N_{PC}$[b] |
|---|---|---|---|---|---|---|---|
| C0α3 | 88 | 0 | 3655 | 3 | 1 | 80 | 0.23 ± 0.01 |
| C0α10 | 88 | 0 | 3655 | 10 | 1 | 82 | 0.50 ± 0.01 |
| C0α30 | 88 | 0 | 3655 | 30 | 1 | 82 | 0.72 ± 0.01 |
| C0α100 | 88 | 0 | 3655 | 100 | 1 | 82 | 0.913 ± 0.003 |
| C3α3 | 124 | 4 | 3200 | 3 | 1 | 120 | 0.21 ± 0.01 |
| C3α10 | 124 | 4 | 3200 | 10 | 1 | 120 | 0.48 ± 0.01 |
| C3α30 | 124 | 4 | 3200 | 30 | 1 | 120 | 0.744 ± 0.006 |
| C3α100 | 124 | 4 | 3200 | 100 | 1 | 120 | 0.922 ± 0.002 |
| C8α3 | 118 | 10 | 3200 | 3 | 1 | 80 | 0.19 ± 0.01 |
| C8α10 | 118 | 10 | 3200 | 10 | 1 | 82 | 0.53 ± 0.01 |
| C8α30 | 118 | 10 | 3200 | 30 | 1 | 94 | 0.81 ± 0.01 |
| C16α3 | 108 | 20 | 3655 | 3 | 1 | 77 | 0.24 ± 0.01 |
| C16α10a | 108 | 20 | 3655 | 10 | 1 | 30 | 0.58 ± 0.03 |
| C16α10b | 108 | 20 | 3200 | 10 | 1 | 102 | 0.47 ± 0.01 |
| C16α10c | 108 | 20 | 3200 | 10 | 0 | 102 | 0.55 ± 0.01 |
| C16α30a | 108 | 20 | 3655 | 30 | 1 | 90 | 0.78 ± 0.01 |
| C16α30b | 108 | 20 | 3200 | 30 | 0.47 | 88 | 0.79 ± 0.01 |
| C31α3a | 88 | 40 | 3655 | 3 | 1 | 108 | 0.37 ± 0.03 |
| C31α3b | 88 | 40 | 3200 | 3 | 0 | 110 | 0.31 ± 0.03 |
| C31α10a | 88 | 40 | 3655 | 10 | 1 | 100 | 0.76 ± 0.02 |
| C31α10b | 88 | 40 | 3202 | 10 | 0.24 | 100 | 0.69 ± 0.02 |
| C31α30 | 88 | 40 | 3655 | 30 | 1 | 88 | 0.92 ± 0.01 |

[a] First number in label notation refers to percent cholesterol, second number refers to activity ratio, and final letter distinguishes multiple trajectories with different lateral distributions of cholesterol; for example, C31α10b refers to the second trajectory performed with 31% cholesterol and α = 10. [b] Average was taken excluding the first 15 ns of simulations, with exceptions of C31α3a and C31α3b where average excludes the first 70 ns of simulations.

contribution to the interaction energies of tail sites.) The "Rosenbluth weight" $W_{new}$ of the new structure is calculated as in ref 47 and compared to the Rosenbluth weight $W_{current}$ calculated for the current chain using energies for $(k-1)$ "dummy" sites generated at each segment. The acceptance probability is calculated as:

$$acc_{DOPC\rightarrow DPPC} = \min\left[1, \alpha\frac{W_{new}}{W_{current}}\right] \text{ or}$$
$$acc_{DPPC\rightarrow DOPC} = \min\left[1, \alpha^{-1}\frac{W_{new}}{W_{current}}\right] \quad (1)$$

where $\alpha = \exp[\beta(\Delta\mu_{DPPC-DOPC})]$ is equal to the ratio of thermodynamic activities (fugacities) of the two lipids. If $acc_{A\rightarrow B}$ equals 1 or is greater than a random number generated on the interval [0,1], the move is carried out; otherwise, the move fails and molecular dynamics proceeds uninterrupted. In case of a successful mutation move, the existing lipid becomes a noninteracting ghost, and the new lipid's interactions are turned on; the newly grown sites on the lipid are assigned new random velocities from a Maxwell−Boltzmann distribution, while the sites common to both lipids are assigned the velocities of the current lipid sites.

The united-atom lipid parameters developed by Berger et al. were used for DPPC[48] and adapted for DOPC. Bond length and bond angles for the double bond of DOPC were taken from the Tieleman group website at the University of Calgary (http://moose.bio.ucalgary.ca/index.php?page=Structures_and_Topologies) with the exception of torsional parameters for carbon−carbon single bonds adjacent to the *cis*-double bonds of DOPC. The parameter set initially used features the potential minimum at $\phi = 180°$, where calculations on small molecular analogues[49] show a local maximum. Use of the parameter set taken from the University of Calgary website for MCMD calculation produced results in contradiction to experiment, that is, the absence of any effect of cholesterol on DPPC/DOPC mixing. Like others,[50] we then recognized the importance of this aspect of the force-field and developed our own parameters using fits to ab initio data. The total relaxed potential energy function for torsion around the C3−C4 bond of (*E*)-2-pentene was calculated at the B3LYP/6-31G** level of theory using the Gaussian 03 electronic structure software suite.[51] From this function, a proper dihedral potential energy function:

$$U(\phi) = 1.97\ \text{kJ/mol}[1+\cos(3\phi)] \quad (2)$$

was used to give a good fit in the barrier region when added to the existing nonbonded Lennard-Jones terms. The potential is similar to that developed by Bachar et al.,[49] although with a slightly lower barrier (3.4 vs 4.3 kJ/mol) at $\phi = 180°$ and with minima at ±126° rather than ±120°. The SPC[52] model for water, and parameters for cholesterol developed by Höltje et al.[53] were used.

To prepare initial configurations, pure DPPC or pure DOPC bilayers were equilibrated, fully solvated, with varying levels of cholesterol and solvent as shown in Table 1. DPPC structures were taken from the end points of previous simulations.[47] DOPC configurations were generated in two steps using the GIMLi 1.0 code: first, an all-DPPC bilayer was converted into an all-POPC bilayer by setting the activity ratio to a small value during a 1 ns simulation. After 5 ns equilibration of the POPC bilayer, the same procedure was used to generate an all-DOPC bilayer, which was then equilibrated for 10 ns. Cholesterol-containing bilayers were prepared by replacing randomly selected lipids (equally divided between the two leaflets) with a "ghost" noninteracting cholesterol and turning on the full cholesterol potential over a 1 ps free energy perturbation trajectory, followed by at least 20 ns of equilibration with cholesterol at 298 K using conventional MD. In two cases (C16α30b and C31α30b), the starting points were intermediate configurations from simulations initiated with 100% DOPC at lower activity ratios (C16α10c and C31α3b, respectively). During MCMD, average acceptance rates for


dx.doi.org/10.1021/ja110425s |*J. Am. Chem. Soc.* 2011, 133, 3625–3634

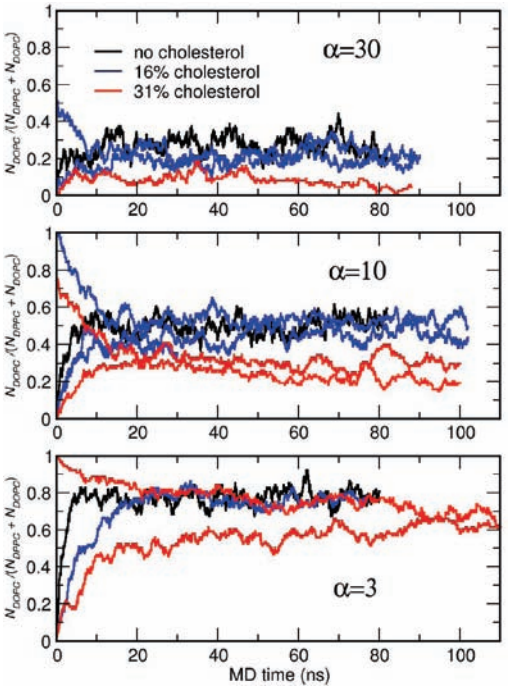


**Figure 1.** Equilibration and fluctuation of PC composition for selected MCMD trajectories.

mutation moves varied between $\sim 2 \times 10^{-5}$ and $\sim 6 \times 10^{-5}$, with lower rates at high cholesterol content. These correspond to average intervals of ~30−100 ps between mutation events for the system as a whole, or an average interval of ~3−10 ns between mutation events for each lipid.

Representative plots of composition versus time are shown in Figure 1 to illustrate equilibration rates and fluctuations during MCMD trajectories. Average compositions reported in Table 1 were calculated excluding the first 15 ns of each trajectory, with the exception of the high-cholesterol, low-activity ratio points (C31α3b and C31α3a) where due to slow convergence the first 70 ns of each trajectory was excluded. Uncertainties reported were calculated using eq 4 of Wang et al.[38] This formula is based on assumptions that mutation events are uncorrelated, that composition is uniform throughout the system, and that environmental factors (e.g., cholesterol conformation) relax quickly relative to changes in composition. Coordinates were saved at 10 ps intervals for analysis. Angle-resolved lateral pairwise distribution plots $g(r,\phi)$ were generated following the convention of Pandit et al.,[29] with the distance $r$ defined as the length of the $XY$-projection of the vector between the oxygen of the cholesterol and the methine CH site of the DPPC or DOPC glycerol backbone (for cholesterol and PC molecules on the same leaflet), and the angle $\phi$ defined with respect to the $XY$-projection of the vector from carbon site 10 to methyl site 19 of cholesterol, that is, with $\phi = 0$ corresponding approximately to the $\beta$ face and $\phi = 180°$ to the α face.

The end points of two trajectories (C16α10b and C16α10c, both at 16% cholesterol with α = 10) were used as starting points for additional MCMD simulation performed under the influence of restraining potentials applied to the tilt angle $\theta$ between the bilayer normal and the cholesterol backbone (defined as the vector connecting the attachment sites of the hydroxyl and the alkyl tail to the ring system). The form of the restraining potential was:

$$U(\theta) = k[1 - \cos[n(\theta - \theta_0)]] \quad (3)$$

Two varieties of angle restraints were used: $k$ = 25 kJ/mol, $n$ = 2, and $\theta_0 = 0$ for a "low tilt" angle distribution, $k$ = 10 kJ/mol, $n$ = 4, and $\theta_0 = 45°$ for a "high tilt" distribution. Independent 40 ns trajectories were generated from each starting point using both sets of angle restraint parameters. Compositions were averaged over the last 30 ns of the trajectories.

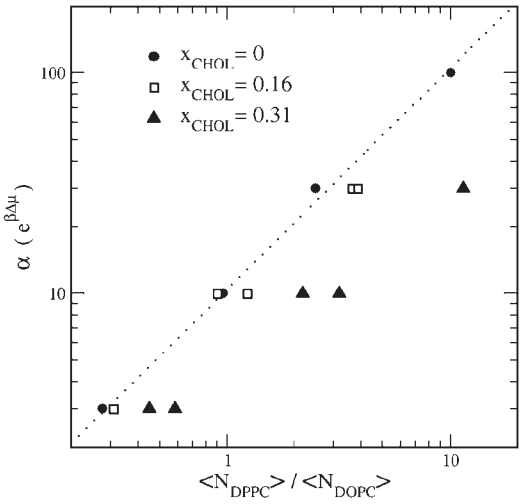


**Figure 2.** Activity ratio α versus average mole ratio at three cholesterol mole fractions, shown on a log−log scale. Dotted line, with slope = 1, is included as a reference for the expected relationship in an ideal mixture.

## RESULTS

**Mixing Thermodynamics in Binary DPPC/DOPC Mixtures.** The success probabilities of the CBMC moves that interchange DPPC and DOPC depend both on the relative stabilities of the two lipids in the local environment and on the activity ratio α defined for the trajectory. The dependence of the mean composition on α in the absence of cholesterol therefore provides insight into the intrinsic thermodynamics of mixing of DPPC and DOPC. If the mixing is ideal, that is, if the lipids' molecular free energies do not depend on the system composition, the average mole ratio will be proportional to the activity ratio. In the absence of cholesterol, deviations from ideal mixture behavior are slight, as shown in Figure 2. No gel-like structures are observed here due to the slow kinetics[54] of the fluid−gel transition.

**Cholesterol Effects on Bilayer Structure.** Increase of cholesterol content in simulated fluid-phase mixtures of DPPC and DOPC leads to increased extension of PC lipid tails as apparent from increasing acyl tail order parameter $S_{CD}$ and bilayer thickness, shown in Figure 3, as is well-known from experiment[55] and simulations.[25,56,57] The effect of cholesterol is weaker for the unsaturated tail DOPC than for the saturated tail DPPC, also consistent with experiment.[58,59]

**Cholesterol Effects on Mixing Thermodynamics.** If mixing were nearly ideal among all three components (that is, if the free energy change associated with adding cholesterol to the bilayer were independent of the bilayer PC composition), then its presence would not affect the mole ratio of DPPC and DOPC at fixed α. Rather, Figures 1 and 2 show that at each value of α, the mole ratio of DPPC to DOPC is higher in the presence of 31% cholesterol than in the binary mixture, indicating that high cholesterol bilayers have a greater affinity (relative to cholesterol-free bilayers) for DPPC than for DOPC. This result is qualitatively consistent with the experimental observation that during phase coexistence in the ternary DPPC/DOPC/cholesterol bilayers, DPPC is enriched in the high-cholesterol LO phase while DOPC is enriched in the low-cholesterol LD phase.[9,11]

Beyond this qualitative trend, it is valuable to be able to test the behavior of the simulation model against the experimental phase behavior of DPPC/DOPC/cholesterol mixtures. Thermodynamic conditions for equilibrium coexistence enable comparison

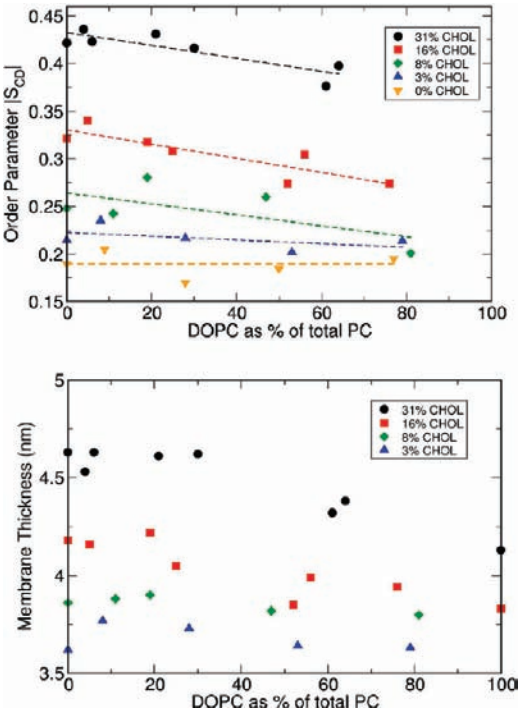


**Figure 3.** Order parameter $|S_{CD}|$ of DPPC acyl tail carbon 9 (top panel) and membrane thickness ($d_{HH}$, distance between peaks of average electron density along bilayer normal) (bottom panel) versus PC content over a range of cholesterol contents.

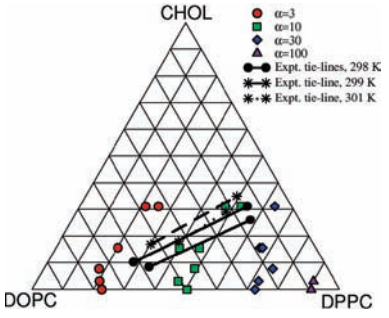


**Figure 4.** Average compositions from semigrand canonical ensemble simulations performed at fixed cholesterol contents and DPPC/DOPC activity ratios α, overlaid with tie lines from experimental literature (ref 11, 298 K; ref 12, 299 K; and ref 60, 301 K) connecting coexisting LD and LO phases in DOPC/DPPC-$d_{62}$/Chol.

of the simulation results (i.e., the relationship between composition and the activity ratio of the two phospholipid components) with experimentally determined tie lines connecting coexisting phases on the ternary phase diagram. At equilibrium, each component in the ternary mixture must have the same chemical potential $\mu$ in the LD phase as it does in the LO phase. The two end points of any tie line therefore must also be characterized by a common difference in chemical potential $\Delta\mu_{DPPC-DOPC}$, or equivalently equal α. Agreement between experiment and simulation is therefore reflected by whether pairs of experimental tie line end points coincide with simulation points generated using the same choice of α. (Further information beyond the reach of the present methods, such as the variation of cholesterol's chemical potential $\mu$ with cholesterol content, would be needed to establish definitively the presence of an LD−LO phase coexistence region and its limits.)

Tie lines for the DOPC/DPPC-$d_{62}$/cholesterol ternary mixture have been reported from experiments by Veatch et al. at 298 K,[11] by Juhasz et al. at 299 K,[12] and by Davis et al. at 301 K.[60] These experimental tie lines are overlaid in Figure 4 with simulation results obtained at constant α and varying cholesterol content. The series at α = 10 runs closest to these tie lines and shows the same trend (increasing DPPC content with increasing cholesterol), but with a smaller shift in PC content with increasing cholesterol. The tendency of high-cholesterol environments to favor DPPC over DOPC is therefore under-predicted by the simulation model relative to experiment. Snapshots generated using the VMD package[61] of structures corresponding to α = 10 at 16% and 31% cholesterol are shown in Figure 5. The randomly generated initial choices for cholesterol placement in the C16α10b structure happened to produce stripe-like domains (an unlikely outcome, but not completely unbelievable; we estimate the probability at ∼1 in $10^3$ or $10^4$), which persisted over the course of the simulation; their presence in Figure 5 should not be taken as evidence of cholesterol self-organization over the trajectory. The cholesterol distributions in C16α10b and C16α10c illustrate that the initial, randomly selected lateral distribution of cholesterol does not converge to an equilibrium distribution; to the extent that the details of cholesterol arrangement may influence the mean balance between PC lipids in the system, variations in original distribution can explain some of the scatter in the simulation points shown in Figure 4.

Beyond the opportunity for comparison with experiment, the influence of cholesterol on the DPPC/DOPC ratio at constant α offers insight into the nature of the driving force for phase separation. Two trends are evident from Figures 2 and 4. First, at the lowest α modeled (i.e., at low DPPC fraction), cholesterol's influence is less pronounced than at higher DPPC fraction. Second, at low and intermediate α, the effect of cholesterol is weak or absent at cholesterol fractions up to 16%, but the DPPC fraction jumps between 16% and 31%. These trends suggest that cholesterol's difference in affinity for the two lipid types is composition-dependent. To test this interpretation, we performed Monte Carlo simulations on two-dimensional square lattice models with only near-neighbor interactions defined. These models were developed solely as a tool to aid in interpretation of the atomistic semigrand canonical simulation results and are not intended to treat all effects comprehensively, in contrast to other simple stand-alone models that have been fruitful in providing mechanistic interpretations.[19,62,63] To mimic the atomistic simulation setup, cholesterol sites were chosen at random and fixed in each simulation. Different fixed distributions of cholesterol were found to produce different equilibrium concentrations of DPPC and DOPC, so multiple trials were performed at each cholesterol fraction to give a sense of the variability associated with the random selection of cholesterol positions.

In the first set of simulations, the energy of a configuration was defined by counting near-neighbor pairs (i.e., eight neighbors, including diagonal neighbors on the square lattice) of different types and multiplying by an interaction energy specific to that pair type. The cholesterol−DOPC interaction was set to a positive value $U_{rep}$ and the cholesterol−DPPC interaction to its negative. Semigrand ensemble simulations with this simple model yield DPPC/DOPC ratios that rise steadily with cholesterol content at constant activity ratio, in contrast to the atomistic

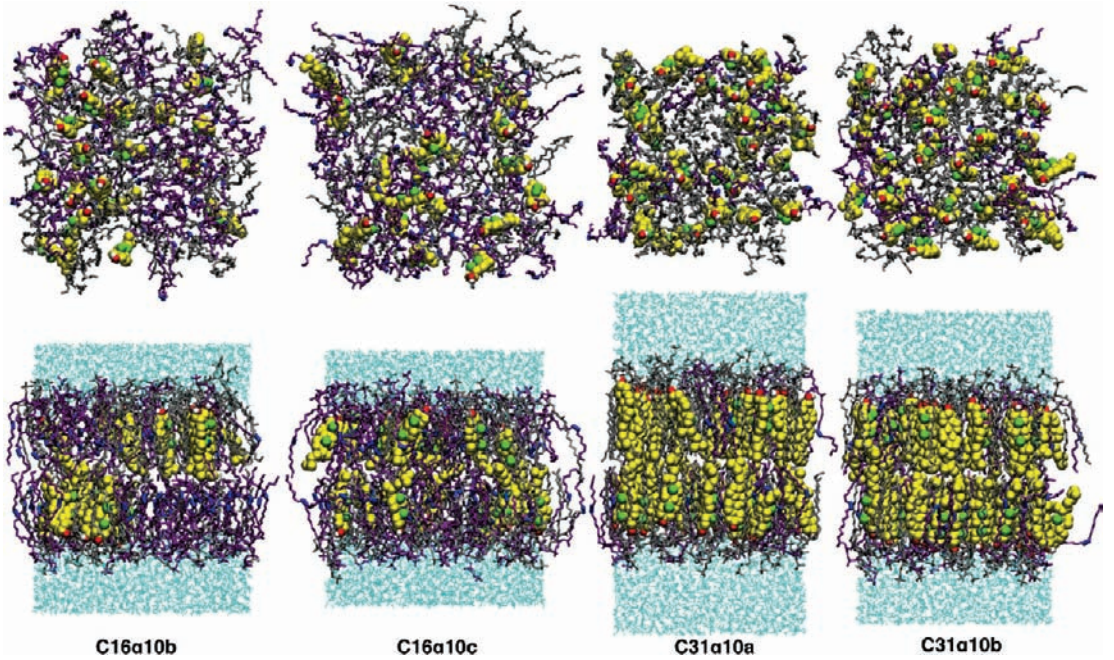


**Figure 5.** Snapshots of final structures of trajectories at activity ratio α = 10 and 16% or 31% cholesterol. Top row shows face view with solvent omitted; bottom row shows side view including water box. Cholesterol is shown in yellow, with $\beta$-face methyl sites in green and hydroxyl in red and white. DPPC is shown in gray, and DOPC in purple with C═C double bonds highlighted in blue.

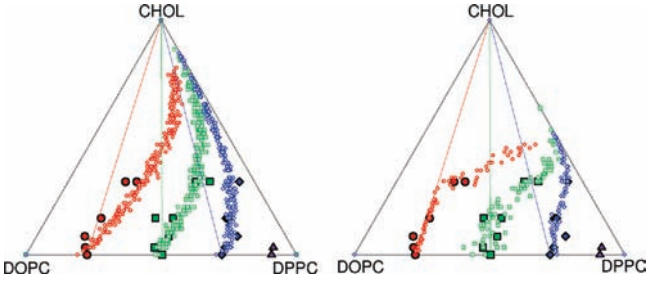


**Figure 6.** Comparison of atomistic simulation results with simple lattice model calculations. Atomistic results are as presented in Figure 4. Small open symbols show mean compositions at three fixed activity ratios and a range of cholesterol contents. Left panel: simple near-neighbor attractions model with $U_{rep}$ = 0.37 $k_BT$. Right panel: cholesterol 2-state model, with $U_{rep}$ = 1.10 $k_BT$ and $U_{SP}$ = 1.61 $k_BT$. Dotted lines show isotherms for a hypothetical ideal mixture.

simulation findings at high DOPC content. A choice of $U_{rep}$ that yielded good agreement with simulation at high DPPC content showed large deviations at low DPPC (see Figure 6, left panel) and vice versa. Adding a second parameter reflecting an energetic preference between DPPC/DPPC and DOPC/DOPC neighbors over DPPC/DOPC neighbors did not improve the agreement (not shown), which is unsurprising given the finding of nearly ideal mixing for the cholesterol-free bilayer.

Lattice MC calculations were next performed with a refined model in which cholesterol may interconvert between two states, "neutral" (N) or "saturated-preferring" (SP). Cholesterol in its N state is assigned identical (zero) energies for interactions with neighboring PC lipids of either type, while SP cholesterol is assigned a repulsive interaction energy $U_{rep}$ for each DOPC neighbor. A fixed energy penalty $U_{SP}$ is defined for the adoption of the "SP" state, but cholesterol−cholesterol interactions are defined so as to promote this state, with an energy penalty set equal to $U_{rep}$ for every N−N neighbor pair, 0.5 $U_{rep}$ for every N−SP pair, and 0 for SP−SP pairs. Such a "two-state" model provides a cooperative or many-body effect, in that the interaction of cholesterol with each neighbor depends on its state, which in turn depends probabilistically on the cholesterol's other neighbors. The pattern of PC content versus cholesterol content at fixed $\Delta\mu_{DPPC-DOPC}$ exhibited by this model was qualitatively similar to the atomistic simulation results: deviation from ideality increased moving toward high cholesterol and high DPPC. Parameters for $U_{SP}$ and $U_{rep}$ were found that could match simulation results satisfactorily, as shown in Figure 6 (right panel). The spread in PC composition calculated from the lattice simulations at any given cholesterol content reflects random variations in lateral distribution patterns of cholesterol, whose tendency to adopt the SP state will depend strongly on its neighbors. We note that the same effect might account for the apparent lack of convergence in PC content between atomistic trajectories initiated with different cholesterol distributions, for instance, C16α10b and C16α10c.

Degree of cholesterol tilt with respect to the bilayer normal was considered as a possible determinant of whether cholesterol is active in discriminating between DPPC and DOPC. As discussed in recent reports,[27,32] this alignment is highly sensitive to overall cholesterol content. Mean tilt angle plotted against PC content in Figure 7 shows that both high cholesterol and high DPPC content favor low cholesterol tilt angles. To test whether the apparent correlation between low tilt angles and cholesterol-induced demixing of DPPC and DOPC is actually a causal relationship, we simulated the effect of perturbing cholesterol tilt through external potentials while maintaining constant activity ratio α. As described in the Methods, the end points of two earlier 100 ns trajectories performed with 16% cholesterol and α = 10 were each used for two further sets of MCMD

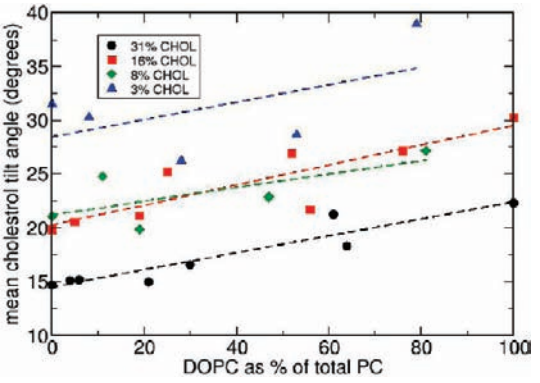


**Figure 7.** Mean cholesterol tilt angle versus cholesterol and DOPC content. Regression lines are included to guide the eye.

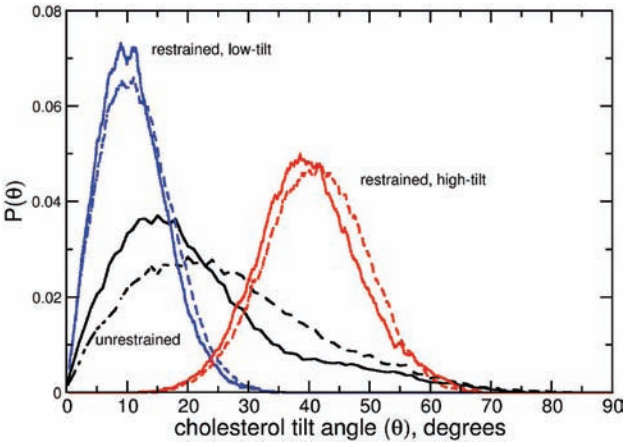


**Figure 8.** Cholesterol tilt angle distributions averaged over MCMD trajectories in the presence and absence of external fields. Solid curves correspond to system "b", and dashed curves to system "c", both at 16% cholesterol and activity ratio α = 10 but with different random lateral distributions of cholesterol.

simulations, one with an applied bias toward low cholesterol tilt angles and the other with an applied bias toward high cholesterol tilt angles. In the absence of an external potential, the cholesterol tilt angle distributions at this cholesterol level are broad, with a significant fraction of molecules tilted at 45° or greater as shown in Figure 8. Moreover, the two sets (b and c) show differences in tilt angle distribution, which (according to the hypothesis) may be related to differences in cholesterol distribution: closer local packing of cholesterol in set b (see Figure 5) is expected to promote alignment and low tilt angles. Simulation at constant α under the influence of artificial tilt-perturbing fields offers an opportunity to check whether bringing the degrees of alignment of both systems to an angle range characteristic of high-cholesterol, high-DPPC systems will promote sorting. Upon application of the external fields, the tilt angle distributions become much more consistent between the two systems. Data presented in Figure 9 show that biasing cholesterol's alignment toward a low tilt angle distribution (with an average tilt ~12°) raises the bilayer's affinity for DPPC over DOPC, confirming that cholesterol's preference for DPPC over DOPC is tilt-dependent. Nonetheless, even when their tilt angle distributions are brought into near agreement through the external restraint potential, differences between the PC contents of the two systems are as

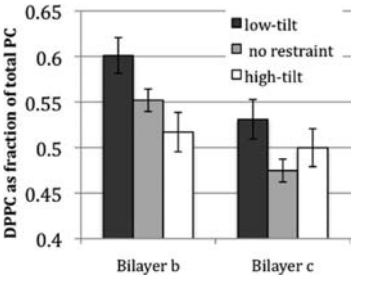


**Figure 9.** Mean DPPC content at α = 10 and 16% cholesterol in the presence of external "low-tilt" or "high-tilt" restraining fields (as defined in the Methods) as compared wto averages for the unperturbed bilayers.

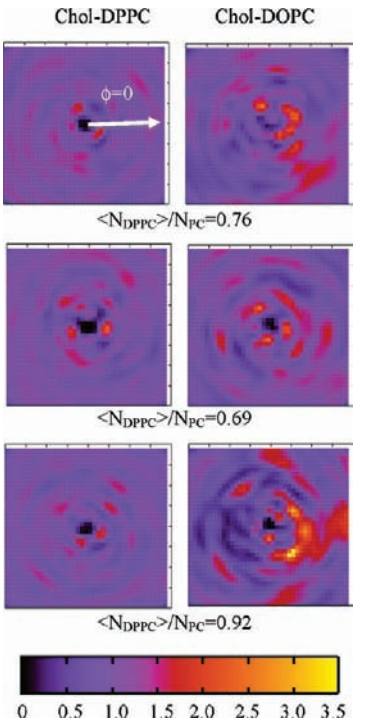


**Figure 10.** Density plots of $g(r,\phi)$ of DPPC and DOPC lipids surrounding cholesterol at high cholesterol and high DPPC (runs C31α10a, C31α10b, and C31α30). Definition of distance and angle coordinates are as defined in Methods; the positive $X$ direction (i.e., $\phi$ = 0) corresponds roughly to the $\beta$ face of cholesterol. All plot areas depict an area of 4.0 × 4.0 nm centered at the cholesterol.

great or greater than the differences between perturbed and unperturbed systems.

As preferences of different lipids for the "rough" and "smooth" faces of cholesterol have been seen in previous simulations and proposed to drive superlattice formation,[30] we have investigated the distribution of DPPC and DOPC as a function of distance and angle around cholesterol. At high cholesterol (31%) and high DPPC (i.e., under conditions of low cholesterol tilt angle, characteristic of the liquid-ordered phase), two features noted in previous reports emerged as shown in Figure 10: a noticeable enrichment of DOPC near the $\beta$ face[29] was evident, and a triangular distribution of neighbor sites around cholesterol.[30] These features were not observed consistently among trajectories performed in other composition regimes, (see Supporting Information, Figure S1, for plots of all trajectories).

## DISCUSSION

In the absence of cholesterol, DPPC and DOPC mix with little or no excess free energy of mixing according to the current simulation results. Near-ideal behavior is somewhat unexpected given that mixtures of these two lipids are known to phase separate into fluid (DOPC-enriched) and gel (DPPC-enriched) phases at the simulation temperature of 298, which is below the transition temperature $T_m$ of DPPC.[64] Previous simulations likewise yielded nearly ideal mixing within the fluid phase (but not the gel phase) of DSPC/DMPC mixtures[37] in the vicinity of a phase boundary. Even within the two-phase region, finite size effects and slow phase transition rates prevent appearance of gel domains and permit the liquid phase to persist metastably as an ideal mixture. This apparent inconsistency can be explained by the large differences between molecular conformation and symmetry in the gel and fluid phases; the strong incompatibility of DOPC with the DPPC gel phase does not necessarily translate to an incompatibility in the context of a disordered fluid phase. By analogy to three-dimensional (bulk) liquids, it is easy to imagine a pair of molecules that form a nearly ideal binary liquid mixture but are immiscible as solids.

The introduction of cholesterol as a third component, with a tendency to prefer DPPC over DOPC in the fluid state, is needed to yield a fluid−fluid phase coexistence. The present simulations offer a direct comparison between observables in an atomistic simulation and experimentally measured features of the LD/LO phase coexistence, the tie line end points. Although the agreement is not quantitative, this result helps to validate the many simulation studies (recently reviewed[23]) aimed at understanding LD/LO phase coexistence by exploring cholesterol's structural and energetic influences on bilayer properties using atomistic force-fields. Uncertainty about whether a force-field's phase behavior matches experiment leaves such studies' applicability open to question. For instance, the preliminary results using a model that neglects the proper treatment[50] of the torsional potential of C−C bonds adjacent to the double bonds casts serious doubt on whether models containing such an error are capable of cholesterol-induced demixing; fortunately, most commonly used force-field parameter sets do not have this error.

Less severe defects in the force-field are likely responsible for the imperfect quantitative correspondence between simulation and experiment. In assessing the quality of agreement with experiment, it is interesting to note the sensitivity of the experimentally measured LD/LO coexistence boundaries to temperature. As apparent in Figure 4, a temperature increase from 298 to 301 K shortens the tie lines enough to nearly coincide with the isotherms obtained from simulation at $\alpha = 10$ and 298 K. A discrepancy of a few degrees in the effective temperature between simulation and experiment is expected for empirical force-fields, except when a characteristic temperature is specifically included in the parametrization; for instance, the gel−fluid transition temperature of the present model for DPPC is estimated to be 6 °C lower than the experimental value in pure bilayers.[54] Given the generally satisfactory level of agreement, this approach can be applied to mechanistic investigations and even predictive studies of perturbations to phase behavior arising from changes to the sterol structure[65,66] or introduction of small molecules with known or inferred effects on membrane rafts.[67]

The lattice simulations show that the atomistic simulation results cannot be interpreted as arising from a simple preference of cholesterol for DPPC over DOPC. Rather, whether cholesterol exhibits this preference depends on the system composition. In seeking a physical justification of this model, we noted that conditions where cholesterol does influence the DPPC/DOPC ratio coincide with conditions where cholesterol exhibits high alignment with the bilayer normal, or low tilt angle $\theta$. As discussed in recent reports,[27,32] this alignment is highly sensitive to overall cholesterol content. At low cholesterol content, isolated cholesterols have significant freedom to rotate within the disordered medium of the hydrophobic bilayer interior, whether composed of saturated or monounsaturated tails. At high concentration, cholesterol is restricted from exploring a full range of orientations, presumably because of steric hindrance involving the rigid cholesterol ring structures. Figure 7 demonstrates this trend and also shows that the degree of order is sensitive to the balance between DPPC and DOPC. As DOPC fraction increases, the mean cholesterol tilt angle increases. The intrinsic skew in DOPC tails makes the molecule less extensible, and therefore less suited to packing among aligned cholesterols, relative to DPPC. (Even in the absence of cholesterol, pure DPPC forms an ordered gel phase with extended tails below 323 K, while pure DOPC remains disordered well below the freezing point of water.) We hypothesize that the "N" state of cholesterol introduced in the simple lattice model, with both phospholipids able to accommodate its presence equally well, corresponds to cholesterol tilted away from the bilayer normal, while the saturated-tail preferring behavior of cholesterol is only evident when cholesterol adopts a low tilt angle.

The absolute control over the molecular potential energy available in simulation studies enabled a direct test of this hypothesis. Applying an aligning field to all cholesterols in the system does result in a shift in PC content toward the saturated PC lipids (Figure 8), showing unambiguously that cholesterol affinity for DPPC over DOPC is greater at lower tilt angles. Whether the tilt dependence is sufficient to explain the full degree of cooperativity evident from the simulation results is more ambiguous. One might expect that upon using an external field to equalize the tilt angle distributions in two systems under conditions of identical cholesterol level, activity ratio, and hydration levels, the DPPC content of the two systems should be equal. Instead, the difference in DPPC content between the systems, which differ significantly with respect to the lateral distribution of cholesterol, as evident in Figure 5, remains greater than the difference between unperturbed and cholesterol-aligned trajectories. The residual discrepancy could suggest that cholesterol's affinity for DPPC over DOPC is more than a simple function of tilt angle and may be influenced by other effects of cholesterol−cholesterol interactions that depend on the details of cholesterol lateral distribution and facial (azimuthal) orientation. Indeed, the previously observed[29] tendency of DOPC to favor the $\beta$ face of cholesterol was evident under low-tilt conditions from angle-dependent radial distribution calculations (Figure 10). On the other hand, even using a lattice model with isotropic, pairwise, near-neighbor interactions, the variation in mean PC content at constant activity ratio associated with different fixed microscopic placements of cholesterol reached ~10% (see Figure 6, left panel), showing that details of the lateral distribution of cholesterol behavior can be important even when facial anisotropy is not a factor.

Because DPPC and DOPC are able to interconvert through mutation moves, they will achieve an equilibrium lateral distribution much more efficiently than if they could only sample new

arrangements through diffusive mixing. In principle, fixed $\Delta\mu_{DPPC-DOPC}$ simulation is well-suited to study the most probable arrangements of the two phospholipids around individual cholesterol molecules (as opposed to the mean composition as a function of cholesterol content), a question that has received much attention in light of the facial asymmetry of cholesterol. Our results (Figure 10) provide tentative support for the proposal[29] that DOPC favors the methylated $\beta$ face; however, determination of the average composition of lipids in specific positions relative to cholesterol is much less precise than finding the average composition of the system as a whole because the corresponding number of lipids sampled is smaller and the statistical noise is greater. The issue is further complicated by the inhomogeneity of the microenvironments around cholesterol, as we have seen that the affinities of cholesterol for different PC lipids change with its tilt angle and perhaps details of its lateral distribution. Unfortunately, because the cholesterol does not interconvert with the phospholipids through mutation (the structural differences make this at best a great technical challenge and at worst impossible), the present simulations are unsuitable to determine the most probable lateral distribution (e.g., random vs superlattice) of cholesterol, whose diffusion is too slow to achieve equilibrium mixing over the course of these trajectories.

## CONCLUSIONS

The ability to perform atomistic simulations at fixed $\Delta\mu_{DPPC-DOPC}$ (difference in chemical potential between DPPC and DOPC) affords a direct computational measure of the relative affinity of these two lipids for high- and low-cholesterol environments. The increase in DPPC content with increasing cholesterol at fixed DPPC/DOPC activity ratio is consistent with the experimental observation that DPPC and cholesterol are enriched in the liquid-ordered phase region of the ternary phase diagram. Through comparison with experimental tie lines, the tendency toward phase separation is demonstrated to be slightly weaker in the simulation model than in experiment. This approach provides a means of validation of the ability of a force-field to model experimental phase behavior and holds promise for predicting and interpreting the qualitative effects of structural or environmental perturbations on the tendency toward phase separation in ternary bilayer mixtures.

Cholesterol concentration effects on PC composition observed at several fixed values of $\Delta\mu_{DPPC-DOPC}$ did not follow the global behavior expected for demixing governed by simple nearest-neighbor attractions. Instead, the relative affinity of cholesterol for DPPC and DOPC is strongly composition-dependent, indicating some cooperative mechanism. We hypothesized that this variation is primarily a function of cholesterol tilt angle with respect to the bilayer normal, which is influenced by cholesterol−cholesterol steric interactions as well as by DPPC/DOPC ratio. This hypothesis was tested using an external potential to perturb the cholesterol tilt angle distribution. Reducing the mean tilt angle did enhance the affinity of cholesterol for DPPC as predicted, although contributing factors to the cooperativity cannot be ruled out.

## ASSOCIATED CONTENT

**Supporting Information.** Complete ref 51 and density plots $g(r,\phi)$ in the format of Figure 10 for all runs. This material is available free of charge via the Internet at http://pubs.acs.org.

## AUTHOR INFORMATION


### Corresponding Author

Email: jkindt@emory.edu

### Present Addresses

[‡]Accelrys, Inc., Burlington, MA 01803.

[⊥]School of Science and Technology, Georgia Gwinnett College, Lawrenceville, GA 30043.


## ACKNOWLEDGMENT

This material is based in part upon work supported by the National Science Foundation under Grant Numbers CHE-0911285 and CHE-0616383. Support from the Cherry L. Emerson Center for Scientific Computation at Emory University is also gratefully acknowledged.

## REFERENCES


(1) Rietveld, A.; Simons, K. *Biochim. Biophys. Acta* **1998**, *1376*, 467.

(2) Dietrich, C.; Bagatolli, L. A.; Volovyk, Z. N.; Thompson, N. L.; Levi, M.; Jacobson, K.; Gratton, E. *Biophys. J.* **2001**, *80*, 1417.

(3) Edidin, M. *Annu. Rev. Biophys. Biomol. Struct.* **2003**, *32*, 257.

(4) Jacobson, K.; Mouritsen, O. G.; Anderson, R. G. W. *Nat. Cell Biol.* **2007**, *9*, 7.

(5) Kaiser, H.-J.; Lingwood, D.; Levental, I.; Sampaio, J. L.; Kalvodova, L.; Rajendran, L.; Simons, K. *Proc. Natl. Acad. Sci. U.S.A.* **2009**, *106*, 16645.

(6) Feigenson, G. W. *Biochim. Biophys. Acta, Biomembr.* **2009**, *1788*, 47.

(7) Feigenson, G. W.; Buboltz, J. T. *Biophys. J.* **2001**, *80*, 2775.

(8) de Almeida, R. F. M.; Fedorov, A.; Prieto, M. *Biophys. J.* **2003**, *85*, 2406.

(9) Veatch, S. L.; Keller, S. L. *Biophys. J.* **2003**, *85*, 3074.

(10) Zhao, J.; Wu, J.; Heberle, F. A.; Mills, T. T.; Klawitter, P.; Huang, G.; Costanza, G.; Feigenson, G. W. *Biochim. Biophys. Acta, Biomembr.* **2007**, *1768*, 2764.

(11) Veatch, S. L.; Soubias, O.; Keller, S. L.; Gawrisch, K. *Proc. Natl. Acad. Sci. U.S.A.* **2007**, *104*, 17650.

(12) Juhasz, J.; Sharom, F. J.; Davis, J. H. *Biochim. Biophys. Acta, Biomembr.* **2009**, *1788*, 2541.

(13) Almeida, P. F. F. *Biochim. Biophys. Acta, Biomembr.* **2009**, *1788*, 72.

(14) Huang, J. Y.; Feigenson, G. W. *Biophys. J.* **1999**, *76*, 2142.

(15) Chong, P. L.-G.; Zhu, W.; Venegas, B. *Biochim. Biophys. Acta, Biomembr.* **2009**, *1788*, 2.

(16) Somerharju, P.; Virtanen, J. A.; Cheng, K. H.; Hermansson, M. *Biochim. Biophys. Acta, Biomembr.* **2009**, *1788*, 12.

(17) Huang, J. *Biophys. J.* **2002**, *83*, 1014.

(18) Pandit, S. A.; Scott, H. L. *Biochim. Biophys. Acta, Biomembr.* **2009**, *1788*, 136.

(19) Tumaneng, P. W.; Pandit, S. A.; Zhao, G. J.; Scott, H. L. *J. Chem. Phys.* **2010**, *132*, 065104.

(20) Risselada, H. J.; Marrink, S. J. *Proc. Natl. Acad. Sci. U.S.A.* **2008**, *105*, 17367.

(21) Perlmutter, J. D.; Sachs, J. N. *J. Am. Chem. Soc.* **2009**, *131*, 16362.

(22) de Meyer, F. J. M.; Benjamini, A.; Rodgers, J. M.; Misteli, Y.; Smit, B. *J. Phys. Chem. B* **2010**, *114*, 10451.

(23) Berkowitz, M. L. *Biochim. Biophys. Acta, Biomembr.* **2009**, *1788*, 86.

(24) Smondyrev, A. M.; Berkowitz, M. L. *Biophys. J.* **2001**, *80*, 1649.

(25) Cournia, Z.; Ullmann, G. M.; Smith, J. C. *J. Phys. Chem. B* **2007**, *111*, 1786.

(26) Vainio, S.; Jansen, M.; Koivusalo, M.; Rog, T.; Karttunen, M.; Vattulainen, I.; Ikonen, E. *J. Biol. Chem.* **2006**, *281*, 348.

(27) Olsen, B. N.; Schlesinger, P. H.; Baker, N. A. *J. Am. Chem. Soc.* **2009**, *131*, 4854.
(28) Pandit, S. A.; Chiu, S. W.; Jakobsson, E.; Grama, A.; Scott, H. L. *Langmuir* **2008**, *24*, 6858.
(29) Pandit, S. A.; Jakobsson, E.; Scott, H. L. *Biophys. J.* **2004**, *87*, 3312.
(30) Martinez-Seara, H.; Rog, T.; Karttunen, M.; Vattulainen, I.; Reigada, R. *PLoS One* **2010**, 5.
(31) Aittoniemi, J.; Niemelä, P. S.; Hyvönen, M. T.; Karttunen, M.; Vattulainen, I. *Biophys. J.* **2007**, *92*, 1125.
(32) Khelashvili, G.; Pabst, G.; Harries, D. *J. Phys. Chem. B* **2010**, *114*, 7524.
(33) Rog, T.; Pasenkiewicz-Gierula, M.; Vattulainen, I.; Karttunen, M. *Biophys. J.* **2007**, *92*, 3346.
(34) Niemelä, P. S.; Ollila, S.; Hyvönen, M. T.; Karttunen, M.; Vattulainen, I. *PLoS Comput. Biol.* **2007**, *3*, e34.
(35) Zhang, Z.; Lu, L.; Berkowitz, M. L. *J. Phys. Chem. B* **2008**, *112*, 3807.
(36) Bennett, W. F. D.; MacCallum, J. L.; Tieleman, D. P. *J. Am. Chem. Soc.* **2009**, *131*, 1972.
(37) Coppock, P. S.; Kindt, J. T. *Langmuir* **2009**, *25*, 352.
(38) Wang, H.; de Joannis, J.; Jiang, Y.; Gaulding, J. C.; Albrecht, B.; Yin, F.; Khanna, K.; Kindt, J. T. *Biophys. J.* **2008**, *95*, 2647.
(39) Jiang, Y.; Wang, H.; Kindt, J. T. *Biophys. J.* **2010**, *98*, 2895.
(40) Yin, F.; Kindt, J. T. *J. Phys. Chem. B* **2010**, *114*, 8076.
(41) Lindahl, E.; Hess, B.; van der Spoel, D. *J. Mol. Model.* **2001**, *7*, 306.
(42) Berendsen, H. J. C.; Postma, J. P. M.; DiNola, A.; Haak, J. R. *J. Chem. Phys.* **1984**, *81*, 3684.
(43) Hess, B.; Bekker, H.; Berendsen, H. J. C.; Fraaije, J. G. E. M. *J. Comput. Chem.* **1997**, *18*, 1463.
(44) Miyamoto, S.; Kollman, P. A. *J. Comput. Chem.* **1992**, *13*, 952.
(45) Essman, U.; Perera, L.; Berkowitz, M. L.; Darden, T.; Lee, H.; Pedersen, L. G. *J. Chem. Phys.* **1995**, *103*, 8577.
(46) Siepmann, J. I.; Frenkel, D. *Mol. Phys.* **1992**, *75*, 59.
(47) de Joannis, J.; Jiang, Y.; Yin, F.; Kindt, J. T. *J. Phys. Chem. B* **2006**, *110*, 25875.
(48) Berger, O.; Edholm, O.; Jähnig *Biophys. J.* **1997**, *72*, 2002.
(49) Bachar, M.; Brunelle, P.; Tieleman, D. P.; Rauk, A. *J. Phys. Chem. B* **2004**, *108*, 7170.
(50) Martinez-Seara, H.; Róg, T.; Karttunen, M.; Reigada, R.; Vattulainen, I. *J. Chem. Phys.* **2008**, *129*, 105103.
(51) Frisch, M. J.; et al. *Gaussian 03*, revision C.01; Gaussian, Inc.: Wallingford, CT, 2004.
(52) Berendsen, H. J. C.; Postma, J. P. M.; van Gunsteren, W. F.; Hermans, J. In *Intermolecular Forces*; Pullman, B., Ed.; D. Reidel: Dordrecht, 1981.
(53) Höltje, M.; Förster, T.; Brandt, B.; Engels, T.; von Rybinski, W.; Höltje, H.-D. *Biochim. Biophys. Acta* **2001**, *1511*, 156.
(54) Coppock, P. S.; Kindt, J. T. *J. Phys. Chem. B* **2010**, *114*, 11468.
(55) Vist, M. R.; Davis, J. H. *Biochemistry* **1990**, *29*, 451.
(56) Smondyrev, A. M.; Berkowitz, M. L. *Biophys. J.* **1999**, *77*, 2075.
(57) Chiu, S.-W.; Jakobsson, E.; Scott, H. L. *J. Chem. Phys.* **2001**, *114*, 5435.
(58) Mills, T. T.; Toombes, G. E. S.; Tristram-Nagle, S.; Smilgies, D.-M.; Feigenson, G. W.; Nagle, J. F. *Biophys. J.* **2008**, *95*, 669.
(59) Pan, J.; Tristram-Nagle, S.; Nagle, J. F. *Phys. Rev. E* **2009**, *80*, 021931.
(60) Davis, J. H.; Clair, J. J.; Juhasz, J. *Biophys. J.* **2009**, *96*, 521.
(61) Humphrey, W.; Dalke, A.; Schulten, K. *J. Mol. Graphics* **1996**, *14*, 33.
(62) Elliot, R.; Szleifer, I.; Schick, M. *Phys. Rev. Lett.* **2006**, *96*, 098101.
(63) Garbes Putzel, G.; Schick, M. *Biophys. J.* **2008**, *95*, 4756.
(64) Schmidt, M. L.; Ziani, L.; Boudreau, M.; Davis, J. H. *J. Chem. Phys.* **2009**, *131*, 175103.
(65) Bacia, K.; Schwille, P.; Kurzchalia, T. *Proc. Natl. Acad. Sci. U.S.A.* **2005**, *102*, 3272.
(66) Carrer, D. C.; Schmidt, A. W.; Knolker, H. J.; Schwille, P. *Langmuir* **2008**, *24*, 8807.
(67) Pakkanen, K.; Salonen, E.; Makela, A. R.; Oker-Blom, C.; Vattulainen, I.; Vuento, M. *Phys. Biol.* **2009**, *6*.